Int. J. Heat Mass Transfer. Vol. 24, pp. 195–203
Pergamon Press Ltd. 1981. Printed in Great Britain

0017-9310/81/0201-0195 $02.00/0

BOUNDARY AND INERTIA EFFECTS ON FLOW AND HEAT TRANSFER IN POROUS MEDIA

K. VAFAI and C. L. TIEN
Department of Mechanical Engineering, University of California,
Berkeley, CA 94720, U.S.A.

(*Received* 7 *February* 1980 *and in revised form* 11 *June* 1980)

Abstract—The present work analyzes the effects of a solid boundary and the inertial forces on flow and heat transfer in porous media. Specific attention is given to flow through a porous medium in the vicinity of an impermeable boundary. The local volume-averaging technique has been utilized to establish the governing equations, along with an indication of physical limitations and assumptions made in the course of this development. A numerical scheme for the governing equations has been developed to investigate the velocity and temperature fields inside a porous medium near an impermeable boundary, and a new concept of the momentum boundary layer central to the numerical routine is presented. The boundary and inertial effects are characterized in terms of three dimensionless groups, and these effects are shown to be more pronounced in highly permeable media, high Prandtl-number fluids, large pressure gradients, and in the region close to the leading edge of the flow boundary layer.

NOMENCLATURE

B, blowing coefficient, v_w/u_C;
c_f, fluid's heat capacity [Ws/kg K];
Da, Darcy number, K/L^2;
d, pore diameter [m];
F, a function used in expressing inertia terms, defined in equation (1);
G, a function used in expressing inertia terms, defined in equation (23);
K, permeability of the porous structure [m^2];
L, horizontal extent of the external boundary [m];
Nu, Nusselt number, defined in equation (30);
P, pressure [N/m^2];
Pr, effective Prandtl number, ν_f/α_e;
Re, Reynolds number, $u_C L/\nu_f$;
Re_K, Reynolds number based on permeability, $u_D\sqrt{K}/\nu_f$;
T, temperature [K];
T_e, free-stream temperature [K];
T_w, external boundary temperature [K];
u, x-component velocity [m/s];
u_C, convective velocity, $-(K/\mu)(\mathrm{d}P/\mathrm{d}x)$ [m/s];
u_D, x-component of the Darcian velocity, [m/s];
U_P, x-component of the pore velocity [m/s];
$\mathbf{V}$, velocity vector [m];
$\mathbf{V}_D$, Darcian velocity vector [m/s];
$\mathbf{V}_P$, pore velocity vector [m/s];
v, y-component velocity [m/s];
v_w, blowing velocity [m/s];
x, spatial coordinate, horizontal [m];
y, spatial coordinate, vertical [m].

Greek symbols

α_e, effective thermal diffusivity, $\lambda_e/\rho_f c_f \delta$ [m^2/s];
γ, porous media shape parameter, $\sqrt{\delta/K}$ [m^{-1}];
δ, porosity of the porous medium;
η, dimensionless vertical length scale, $y/(x/PrRe\sqrt{Da})$;
θ, dimensionless temperature, $(T-T_w)/(T_e-T_w)$;
λ_e, effective thermal conductivity [W/mK];
μ_f, fluid's dynamic viscosity [kg/ms];
ν_f, fluid's kinematic viscosity [m^2/s];
ξ, dimensionless horizontal length scale, x/L;
ρ_f, fluid's density [kg/m^3];
Φ, boundary parameter, $(Pr/\gamma L)^2$;
Ψ, inertia parameter, $GRe/\gamma^2 L$;
Ω, blowing parameter, BPr.

Other

$\langle\ \rangle$, denotes the 'local volume average' of a quantity.

1. INTRODUCTION

SINCE the early work of Darcy in the nineteenth century, extensive investigations have been conducted on flow and heat transfer through porous media, covering a broad range of different fields and applications such as ground-water hydrology, petroleum reservoir and geothermal operations, packed-bed chemical reactors, transpiration cooling, and building thermal insulation. Most analytical studies deal primarily with the mathematical formulation based on Darcy's law, which neglects the effects of a solid boundary or the inertial forces on fluid flow and heat transfer through porous media [1–3]. These effects are expected to become more significant near the boundary and in high-porosity media, thus causing the application of Darcy's law to be invalid [4–5]. Moreover, recent upsurge of utilizing high-porosity media in contemporary technology provides further impetus for a thorough understanding of the boundary and inertia effects. In spite of their common presence,

however, relatively little attention has been given to the study of these effects. Brinkman's [6] and Muskat's [7] work form the cornerstone of these boundary and inertial investigations. Brinkman accounted for the presence of a solid boundary through adding a viscous term to Darcy's law, while Muskat included a velocity-squared term in Darcy's law to account for the inertial forces. Unfortunately their work lacks a rigorous analytical basis and does not consider boundary and inertia effects simultaneously.

The present work applies the volume-averaging technique [8, 9] to the fundamental flow and energy equations in a porous medium. Due to application of this averaging technique, certain details of information is lost, thus requiring the use of well-established empirical relations in setting up the 'macroscopic' (over a small volumetric element in the porous medium) governing equations. The presence of an external solid boundary leads to a momentum boundary layer concept for flow in the porous medium. Numerical results for the boundary-layer solution exhibit clearly the boundary and inertial effects on heat transfer under various flow conditions. These effects are conveniently expressed in terms of three dimensionless parameters, which allow a simple characterization scheme for interpreting the applicability of Darcy's law to various problems of flow and heat transfer in porous media. The present analysis is under the assumption of a constant-porosity medium, thus neglecting the effect of possible porosity variations near the wall as often discussed in packed-sphere beds [5].

2. FORMULATION

The analysis of flow and heat transfer is usually based on the transport equations resulting from the differential balance laws, and to predict global effects such as flow resistance or heat flux from a given object requires detailed information of the surrounding velocity and temperature fields. This information is extracted from the solution of the associated transport equations, subject to the pertinent boundary conditions. When flow through a complex structure such as a porous medium is involved, these equations are still valid inside of the pores, but the geometric complexity prevents general solutions of the detailed velocity and temperature fields. Instead, some form of the 'macroscopic' balance equations based on the average over a small volumetric element must be employed. A common practice is to replace the 'microscopic' momentum and energy equations by the corresponding 'macroscopic' equations with the help of some well-established empirical relations.

Empirical relations

It is well known that in flow through a porous medium the pressure drop caused by the frictional drag is directly proportional to velocity for low speed flow. This is the familiar Darcy's law which relates the pressure drop and velocity in an unbounded porous medium. At higher velocities, inertial effects become appreciable, causing an increase in the form drag. Experimental observations do indicate that the pressure drop in the bulk of a porous medium is proportional to a linear combination of flow velocity and square of the flow velocity. The square term is caused by the inertial effects offered through the solid matrix. This can be formulated for steady, incompressible flow as

$$\frac{\mathrm{d}P}{\mathrm{d}x} = -\frac{\mu_f}{K}u_D - \frac{F(K, Re_K, \text{Geometry})}{\sqrt{K}}\rho_f u_D^2 \quad (1)$$

where P is pressure, x the flow direction, μ_f the fluid viscosity, K the permeability, u_D the Darcian fluid velocity in the x-direction and ρ_f the fluid density. The function $F(K, Re_K, \text{Geometry})$ depends upon the Reynolds number, $Re_K = \rho_f u_D \sqrt{K}/\mu_f$, as well as the microstructure of the porous medium. The given functional dependence of F can be deduced from a number of empirical results [7, 10–12]. In equation (1), u_D represents an averaged velocity over a gross cross-section of the porous medium. However, a more descriptive quantity for the flow field in a porous medium is the pore velocity u_P which represents the local average velocity of the fluid in the pores. The relation between u_p and u_D can be readily established from the flow continuity considerations

$$u_D = \delta u_P. \quad (2)$$

Casting equation (1) in terms of the local pore velocity u_P and then generalizing it as a vectorial representation yield:

$$\nabla P = -\frac{\mu_f \delta}{K}\mathbf{V}_P - F\rho_f \delta^{3/2}\gamma(\mathbf{V}_P \cdot \mathbf{V}_P)\mathbf{J} \quad (3)$$

where δ is the porosity, $\mathbf{V}_P$ is the pore velocity vector, $\gamma = \sqrt{(\delta/K)}$ and $\mathbf{J} = \mathbf{V}_P/|\mathbf{V}_P|$ is a unit vector oriented along the pore velocity vector. Equation (3) can be regarded as an empirically based local volume average of the 'microscopic' momentum equation in an unbounded porous medium, with $\mathbf{V}_P$ being the local volume average velocity vector.

The empirically based energy equation in a porous medium, often mistaken as an exact equation, is given by

$$\rho_f c_f \mathbf{V}_D \cdot \nabla T = -\nabla \cdot (-\lambda_e \nabla T) \quad (4)$$

where c_f is the fluid heat capacity, $\mathbf{V}_D$ the Darcian velocity vector, T the temperature, and λ_e the effective conductivity of the porous medium saturated with a stagnant fluid. The concept of λ_e has been widely used and studied [13]. The velocity vector $\mathbf{V}_D$ used in equation (4) represents a global average value of the velocity in a porous medium while the equation itself is an energy balance on a local differential element. Therefore, it seems more appropriate using the pore velocity representing the local average value of the fluid velocity in equation (4). There follows for

constant-porosity media

$$\rho_f c_f \mathbf{V}_P \cdot \nabla T = -\nabla \cdot [-(\lambda_e/\delta)\nabla T]. \quad (5)$$

Equation (5) can be considered as an empirically based local volume average of the 'microscopic' energy equation in a porous medium.

After establishing the appropriate forms of the empirical momentum and energy equations in a porous medium, a more rigorous approach is considered next. The most logical form appears to be the one established from the local volume average of the differential balance laws [8, 9].

Local volume averaging analysis

The averaging process is accomplished by associating with every point in the porous medium a small volume V bounded by a closed surface A. The minimum size of V will be discussed later. Let V_f be that portion of V containing the fluid, and let A_{sf} be the area of pore walls contained within V_f. The local volume average of a quantity Ψ associated with the fluid is thus defined as

$$\langle \Psi \rangle \equiv \frac{1}{V} \int_{V_f} \Psi \, dV. \quad (6)$$

Using the 'volume average of a divergence' theorem [14, 15], the local volume averages of the differential balance laws for an incompressible, steady flow through a porous medium can be established as [9, 14]

$$\nabla \cdot \langle \mathbf{V} \rangle = 0 \quad (7)$$

$$\rho_f \langle (\mathbf{V} \cdot \nabla)\mathbf{V} \rangle = -\nabla \langle P \rangle + \mu_f \nabla^2 \langle \mathbf{V} \rangle + \mathbf{r} \quad (8)$$

$$\rho_f c_f \langle \mathbf{V} \rangle \cdot \nabla \langle T \rangle = -\nabla \cdot \chi \quad (9)$$

where

$$\mathbf{r} = -\frac{1}{V} \int_{A_{sf}} S \cdot d\mathbf{A} \quad (10)$$

$$\chi = \beta \nabla \langle T \rangle + \zeta |\nabla \langle T \rangle| \langle \mathbf{V} \rangle \quad (11)$$

S being the fluid's stress tensor, and β and ζ are complex functions of δ, c_f, λ_f (the fluid thermal conductivity), λ_s (the solid matrix thermal conductivity), $|\langle \mathbf{V} \rangle|$, $|\nabla \langle T \rangle|$ and $\langle \mathbf{V} \rangle \cdot \nabla \langle T \rangle$ [14]. Equations (7)–(9) are 'macroscopic' conservation equations for fluid mass, momentum, and energy, respectively. The body-force term $\mathbf{r}$ is caused by the micropore structure and χ can be considered as an effective heat flux vector of the porous medium and the fluid. It should be noted that the stated energy equation requires the additional assumption of small temperature differences between the fluid and the solid matrix, which is generally valid except for a highly conducting solid matrix or when encountering high fluid velocities.

Due to the volume-averaging process, some information is lost, thus requiring supplementary empirical relations for $\mathbf{r}$ and χ. It should be noted that the empirical information to be employed here concerns specific physical terms in the fundamental transport equations and is quite different from the global empirical relations as given in equations (3) and (5).

Consider first the body-force term $\mathbf{r}$, which is in effect a measure of the flow resistance offered by the solid matrix. Since the pressure gradient as given in equation (3) can also be interpreted as a measure of the same resistance to flow in the bulk of the porous medium, $\mathbf{r}$ can be inferred from equation (3) to be

$$\mathbf{r} = -\frac{\mu_f \delta}{K} \langle \mathbf{V} \rangle - F \rho_f \delta^{3/2} \gamma (\langle \mathbf{V} \rangle \cdot \langle \mathbf{V} \rangle) \mathbf{J}. \quad (12)$$

The heat flux term χ can be established through comparing the analytical volume-averaged energy equation (9) with the corresponding empirical volume-averaged equation (5) as

$$\chi = -\frac{\lambda_e}{\delta} \nabla \langle T \rangle. \quad (13)$$

The above reasoning, although not exact, provides good justification for neglecting the second term of the right-hand side of equation (11).

Using equations (12) and (13) in equations (8) and (9) renders the following governing equations:

$$\Lambda_I \langle (\mathbf{V} \cdot \nabla)\mathbf{V} \rangle = -\nabla \langle P \rangle^f + \Lambda_B \nabla^2 \langle \mathbf{V} \rangle - \Lambda_P \langle \mathbf{V} \rangle - \rho_f F \sqrt{(\delta)} \gamma [\langle \mathbf{V} \rangle \cdot \langle \mathbf{V} \rangle] \mathbf{J} \quad (14)$$

$$\langle \mathbf{V} \rangle \cdot \nabla \langle T \rangle = \alpha_e \nabla^2 \langle T \rangle \quad (15)$$

where

$$\Lambda_I = \rho_f/\delta, \quad \Lambda_B = \mu_f/\delta, \quad \Lambda_P = \mu_f/K, \quad \alpha_e = \lambda_e/\rho_f c_f \delta \quad (16)$$

and

$$\langle P \rangle^f = \frac{1}{V_f} \int_{V_f} P \, dV.$$

The term $\langle P \rangle^f$ represents the pressure read off a pressure gauge, as the gauge actually measures the average pressure inside the fluid, rather than over the fluid and solid volume. Note that $\langle P \rangle = \delta \langle P \rangle^f$.

Some physical insight can be gained in equation (14) by considering the limiting case of one-dimensional low speed flow. For this case, the equation in the non-dimensional form is

$$-\frac{d\langle \bar{P} \rangle^f}{d\xi} + \frac{Da}{\delta} \nabla^2 \langle \bar{u} \rangle - \langle \bar{u} \rangle = 0 \quad (17)$$

where $\bar{u} = u/u_C$, $\xi = x/L$, $\langle \bar{P} \rangle^f = \langle P \rangle^f / (\mu_f u_C L/K)$, $Da = K/L^2$, and L is a characteristic length. Equation (17) should reduce to the regular viscous flow equation and Darcy's law in the limits of high and low porosities, respectively. For the high-porosity regime, Emersleben's fiber-theory [1] correlates K and δ, reducing equation (17) to the viscous equation, while at low porosities, Carman theory [1] relates K and δ, resulting in Darcy's law.

3. BOUNDARY-LAYER CONCEPT

The effects of a solid boundary on flow and heat

transfer in a porous medium originate from vorticity diffusion caused by the boundary frictional resistance. This resistance is additional to the bulk frictional drag induced by the solid matrix as characterized by Darcy's law. The boundary effects are best described in terms of a new concept of the momentum boundary layer, in which the above two resistances are of the same order. The basic boundary layer characteristic of large velocity gradients normal to the boundary is also retained in the above concept. This boundary layer, however, differs from the conventional one in that the latter characterizes a balance between viscous and inertial effects.

Momentum boundary-layer characteristics

An order-of-magnitude analysis on equation (14) reveals that the momentum boundary-layer thickness is of the order of $\sqrt{(K/\delta)}$. Table 1 presents the calculated values of this thickness for flow of some common fluids with different thermophysical properties in typical high-porosity media. The permeabilities were estimated on the basis of Emersleben's fiber theory [1] from the typical pore diameters in commercial low-density Foametals. As shown in Table 1, the boundary viscous effects are confined in such a thin layer, that it makes experimental observations very difficult. For this reason, existing experimental information have been primarily limited to gross effects such as pressure drop and flow rate correlations. In most flow experiments, the boundary effects on the flow rate are indeed insignificant. But, as to be shown later, neglecting these effects may lead to appreciable errors in heat transfer computations. In particular these errors will become more pronounced when all or most of the thermal boundary layer falls within the momentum boundary layer.

The same analysis also shows that the term $\langle(\mathbf{V}\cdot\nabla)\mathbf{V}\rangle$ responsible for the boundary-layer growth is significant only over a length of the order of (Ku_C/ν). Table 1 indicates that this quantity (Ku_C/ν) is small for most practical situations except for flow of low dynamic-viscosity fluids in a highly permeable medium. Therefore, beyond the short developing region the momentum equation reduces to

$$\Lambda_B\nabla^2\langle\mathbf{V}\rangle - \Lambda_P\langle\mathbf{V}\rangle - \rho F\sqrt{(\delta)}\gamma \times [\langle\mathbf{V}\rangle\cdot\langle\mathbf{V}\rangle]\mathbf{J} - \nabla\langle P\rangle^f = 0 \quad (18)$$

where ∇^2 does not include the component in the flow direction. This fully developed momentum boundary layer is a unique feature of the flow, in contrast with the ever-developing boundary layer in conventional flow.

Minimum volume for volume averaging

To study flow and heat transfer inside the momentum boundary layer, care should be exercised in dealing with the averaging process. The thinness of the boundary layer raises fundamental questions in the interpretation of the average quantities involved. This may be resolved by introducing a technique for choosing the proper size of the volume element associated with the averaging procedure. The minimum size of the volume element is discussed here with specific reference to the two-dimensional flow to be considered later in detail.

The minimum volume should be large enough to yield statistically meaningful averages of relevant physical quantities. Such a meaningful average is achieved by associating a thin cylindrical volume infinitely extended, with its axis passing through each point of interest and perpendicular to the flow direction. Since special emphasis is placed on the points close to the boundary, this technique becomes particularly attractive in providing meaningful interpretation for those points. It is evident that the above choice of the volume element applies only to two-dimensional problems in a strict sense. This demonstrates that a formulation like Brinkman's is applicable only for two-dimensional problems.

4. ANALYSIS OF TWO-DIMENSIONAL BOUNDARY LAYER

To illustrate the importance of the momentum boundary layer and its effects on heat transfer, analysis is made for an incompressible, two-dimensional flow through a porous medium confined by an external boundary as shown in Fig. 1. Dimensional analysis of the energy equation (15) indicates that the thermal boundary-layer thickness inside the momentum boundary layer is of the order of $(x/PrRe\sqrt{Da})$, where Pr is the effective Prandtl number (ν_f/α_e) and Re the Reynolds number defined by (u_CL/ν_f). It should be emphasized that the thermal boundary layer, unlike the momentum boundary layer, grows continuously

Table 1. Characteristics of typical momentum boundary layers in high porosity porous media

Fluid	ν (m²/s)	δ	d (m)	K (m²)	u_C (m/s)	$\sqrt{K}/\delta$ (m)	Ku_C/ν (m)
Air	1.5×10^{-5}	0.98	10^{-4}	10^{-6}	0.1	10^{-3}	6.6×10^{-3}
Air	1.5×10^{-5}	0.98	10^{-3}	10^{-4}	0.1	10^{-2}	0.6
Water	1.5×10^{-6}	0.98	10^{-4}	10^{-6}	0.1	10^{-3}	6.0×10^{-2}
Water	1.5×10^{-6}	0.98	10^{-3}	10^{-4}	0.1	10^{-2}	6.6
Light oil	9.5×10^{-5}	0.98	10^{-4}	10^{-6}	0.1	10^{-3}	10^{-3}
Light oil	9.5×10^{-5}	0.98	10^{-3}	10^{-4}	0.1	10^{-2}	0.1
Engine oil	9.0×10^{-4}	0.98	10^{-4}	10^{-6}	0.1	10^{-3}	10^{-4}
Engine oil	9.0×10^{-4}	0.98	10^{-3}	10^{-4}	0.1	10^{-2}	6.0×10^{-2}

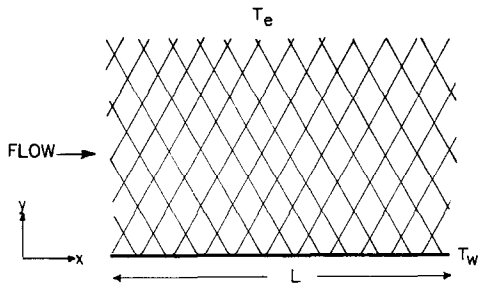

FIG. 1. Flow through a porous medium confined by an external boundary.

with x. This suggests the use of coordinate transformation so that convenient grid selection can be employed later to achieve efficient and accurate numerical computation of flow and thermal boundary layers. The governing momentum and energy equations, (18) and (15) are thus expressed as

$$\Phi\frac{\Gamma^2}{\xi^2}\frac{\partial^2\langle\bar{u}\rangle}{\partial\eta^2} - \Psi\langle\bar{u}\rangle^2 - \langle\bar{u}\rangle + 1 = 0 \quad (19)$$

$$\xi^2\langle\bar{u}\rangle\frac{\partial\langle\theta\rangle}{\partial\xi} - (\langle u\rangle\eta\xi - \Omega\Gamma\xi) \times\frac{\partial\langle\theta\rangle}{\partial\eta} = \kappa\Gamma^2\frac{\partial^2\langle\theta\rangle}{\partial\eta^2} \quad (20)$$

where

$$\xi = x/L, \qquad \eta = y/(x/PrRe\sqrt{Da}) \qquad (21)$$
$$\bar{u} = u/u_C, \qquad \theta = (T - T_w)/(T_e - T_w)$$

$$\Phi = (Pr/\gamma L)^2, \quad \Psi = GRe/\gamma^2 L, \quad \Omega = BPr,$$
$$\kappa = Pr/Re, \quad \Gamma = Re\sqrt{Da} \quad (22)$$

$$G = F(K, Re_K, \text{Geometry})\delta^{3/2}\gamma. \quad (23)$$

Here, y is the normal coordinate, L horizontal extent of the boundary, T_w the boundary temperature and T_e the free-stream temperature. The effect of boundary blowing or suction is also incorporated in the analysis and is characterized by the blowing coefficient B defined by $B \equiv v_w/u_C$ where v_w is the surface blowing velocity. An integral balance on the momentum boundary layer shows that when $B \ll (1/Re\sqrt{Da})$ blowing has negligible effects on the pressure drop as compared to that due to either boundary resistance or the bulk resistance, and thus the momentum equation (19) needs no modification. Blowing, however, does affect heat transfer through additional convection normal to the boundary as shown in equation (20).

The corresponding boundary conditions are

$$\eta = 0, \quad \langle\bar{u}\rangle = 0, \quad \langle\bar{v}\rangle = v_w/u_C, \quad \langle\theta\rangle = 0 \quad (24)$$

$$\eta \to \infty, \quad \langle\bar{u}\rangle = [-1 + \sqrt{(1 + 4\Psi)}]/2\Psi, \quad \langle\theta\rangle = 1 \quad (25)$$

The free-stream boundary condition on the velocity is obtained from the solution of equation (19) neglecting the first term.

Before embarking on a numerical analysis of equations (19) and (20), it is of interest to consider first the limiting case of no blowing and negligible boundary and inertia effects, which allows a closed-form solution. For this case, equations (19) and (20) reduce to

$$\langle\bar{u}\rangle = 1 \quad (26)$$

$$\xi^2\langle\bar{u}\rangle\frac{\partial\langle\theta\rangle}{\partial\xi} - \langle\bar{u}\rangle\eta\xi\frac{\partial\langle\theta\rangle}{\partial\eta} = \kappa\Gamma^2\frac{\partial^2\langle\theta\rangle}{\partial\eta^2}. \quad (27)$$

In conjunction with the appropriate boundary conditions, equation (27) can be solved to yield an analytical solution for the temperature distribution

$$\langle\theta\rangle = \frac{2}{\sqrt{\pi}}\int_0^{\frac{\eta}{2}\sqrt{(\frac{Re}{Pr}\xi)}} e^{-w^2}\,dw = \text{erf}\left[\frac{\eta}{2}\sqrt{\left(\frac{Re}{Pr}\xi\right)}\right] \quad (28)$$

which is of the same general form as the solution of transient heat conduction or the temperature solution in a slug flow. The above solution shows that the thermal boundary layer thickness, δ_T is given by

$$\delta_T \simeq 7\sqrt{\frac{xL}{PrRe}}. \quad (29)$$

This reaffirms the expected result that any increase in the convected energy compared to that by conduction leads to a thinner thermal boundary layer. The exact analytical solution for the case without blowing, boundary and inertia effects will be used as the basis of comparison with the corresponding numerical solution to assess the accuracy of the numerical scheme.

All numerical results are based on the assumption that an external boundary is insulated up to the point where the momentum boundary layer is fully developed. Furthermore, the value 0.07 of the function F is taken as that of a Foametal with no free fiber ends within the body of the porous medium [10]. The computed shapes of momentum and thermal boundary layers are displayed in Fig. 2 for light oil and water with a given set of relevant physical parameters. The γ value corresponds to a permeability of 10^{-6} for both water and light oil. The value of $Re\sqrt{Da}$ for either fluid corresponds to the pressure gradient given in Table 2.

Effects of the boundary on the velocity field as seen in Fig. 2 are indeed confined in a thin region and thus difficult to observe experimentally. However, the wall heat flux, a convenient quantity for experimental measurements, provides an indirect method to detect such effects. The Nusselt number, which characterizes the wall heat flux, is expressed as

$$Nu = -\left.\frac{\partial\langle T\rangle}{\partial y}\right|_{y=0}\Big/\frac{(T_w - T_e)}{L} = \frac{Pr}{\xi}\left.\frac{\partial\langle\theta\rangle}{\partial\eta}\right|_{\eta=0}. \quad (30)$$

5. RESULTS

A numerical scheme based on the linearized equation (19) has been developed using upwind differencing in the ξ-direction and an implicit routine in the η-direction. The linearization scheme for equation (19)

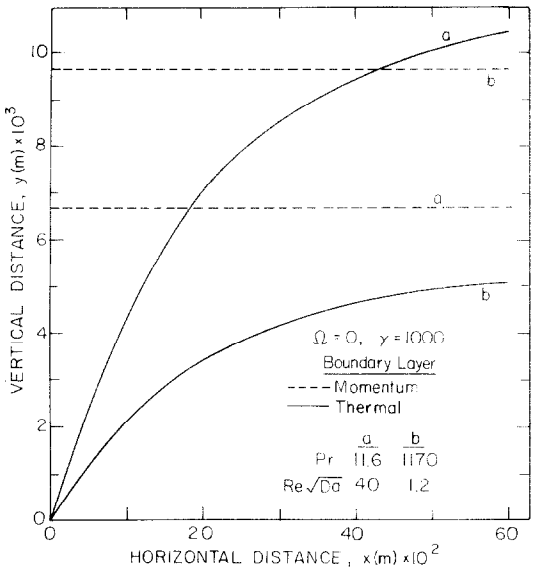

FIG. 2. Computed shapes of the momentum and thermal boundary layers.

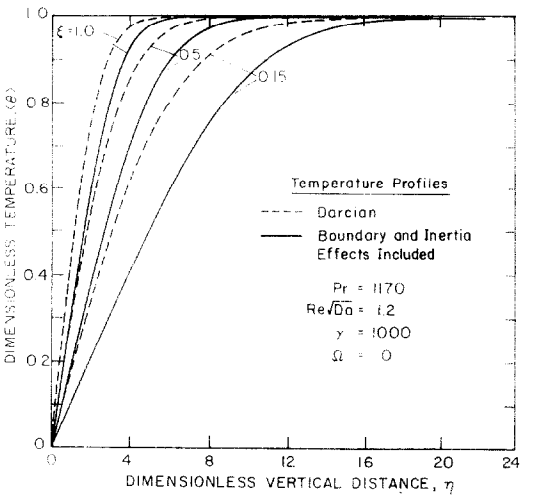

FIG. 3. The non-dimensional temperature profiles for cases without blowing.

has been checked by increasing the number of iterations used for convergence. To trace and cover the entire momentum and thermal boundary layers, variable grid sizes have been employed to account for the thermal boundary-layer growth, followed by updating the velocity distribution in each of the new grid systems. The accuracy of the finite-difference has been tested through increasing the number of grid points. It should also be noted that the boundary-layer solutions here can be used for confined geometries such as channel flow because of the small thickness and the slow growth of the thermal boundary layer.

Presented in Figs. 3 and 4 are the temperature profiles for light oil and water for certain ranges of the system parameters. Figures 5 and 6 show a comparison between the Nusselt numbers obtained for the two cases shown in Figs. 3 and 4, along with the percentage difference between the corresponding Nusselt numbers. The error resulted from omitting boundary and inertial effects, as indicated in Figs. 5 and 6, decreases with increasing downstream distance. This is

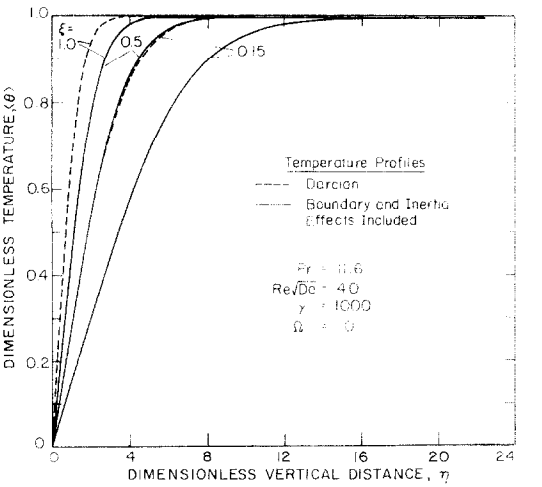

FIG. 4. The non-dimensional temperature profiles for cases without blowing.

anticipated since the thermal boundary layer grows with x. Figures 7 and 8 demonstrate the blowing effects on temperature profiles and Nusselt numbers corresponding to the same parameters used in Figs. 3 and

Table 2. Boundary and inertia effects on the average Nusselt number for some common fluids of different thermophysical properties

Fluid	Pr	K (m^2)	Pressure gradient (N/m^3)	$L \times 10^2$ (m)	Φ	Ψ	Ω	Percentage error on the average Nusselt number
Air	0.7	10^{-6}	10^{1}	60	1.4×10^{-6}	3.0	0	52
Air	0.7	10^{-4}	10^{-1}	60	1.4×10^{-4}	30.0	0	172
Water	11.6	10^{-6}	10^{2}	60	3.6×10^{-4}	2.9	0	72
Water	11.6	10^{-4}	10^{-1}	60	3.6×10^{-2}	2.9	0	112
Light oil	1170	10^{-6}	10^{4}	60	3.7	8.6×10^{-2}	0	58
Light oil	1170	10^{-4}	10	60	3.7×10^{2}	8.6×10^{-2}	0	95
Engine oil	10400	10^{-6}	10^{6}	60	2.9×10^{2}	4.8×10^{-2}	0	90
Engine oil	10400	10^{-4}	10	60	2.9×10^{4}	4.8×10^{-1}	0	175

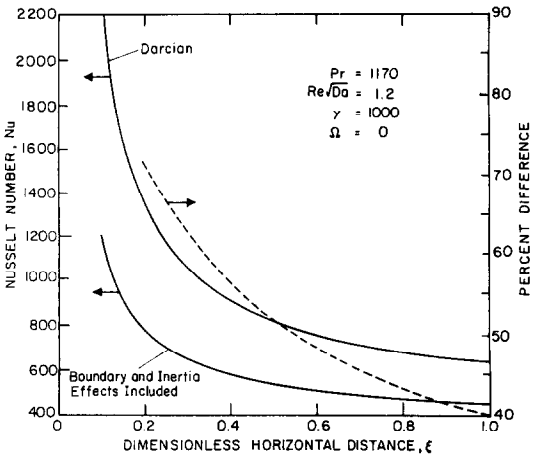

FIG. 5. Comparison between the Nusselt numbers for the two cases in Fig. 3.

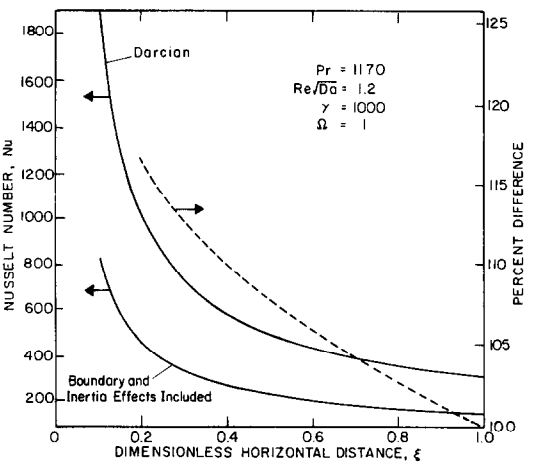

FIG. 8. Comparison between the Nusselt numbers for the two cases in Fig. 7.

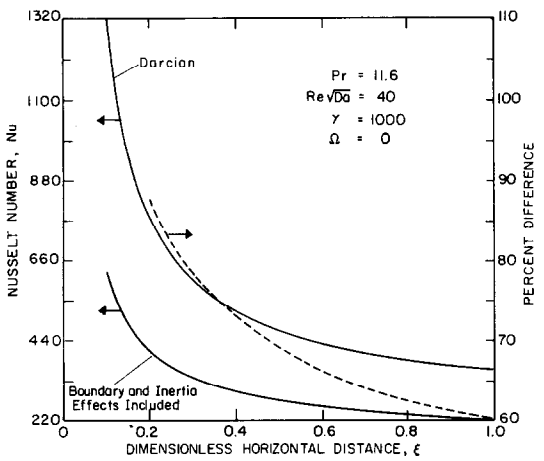

FIG. 6. Comparison between the Nusselt numbers for the two cases in Fig. 4.

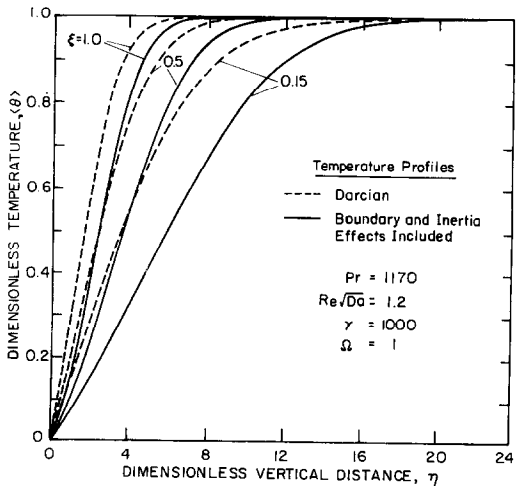

FIG. 7. The non-dimensional temperature profiles for cases with blowing.

5. It can be seen that even small amounts of blowing enhance greatly the boundary effects, thereby increasing further the error involved through neglecting these effects. Inversely, suction lessens the boundary effects.

The results obtained from equations (19)–(25) can be presented in the following functional form

$$Nu \leqq Nu(\Phi, \Psi, \Omega, \kappa, \Gamma). \tag{31}$$

For any set of porous media having similar microstructures, κ and Γ can be shown to be strong functions of Φ and Ψ in the ranges of concerned permeabilities and Reynolds numbers. Therefore, equation (31) becomes

$$Nu = Nu(\Phi, \Psi, \Omega). \tag{32}$$

The percentage error involved in calculating the average Nusselt number along an external boundary using Darcy's law instead of accounting for boundary and inertial effects can then be calculated for each fixed Ω. These errors for four different fluids covering a wide range of Prandtl numbers are given in Table 2 under specified sets of operating conditions. For the case of no blowing ($\Omega = 0$), Fig. 9 presents an error map for the average Nusselt number as a function of the inertial parameter Ψ, and the boundary parameter Φ, illustrating the ranges of applicability of Darcy's law. Results obtained from Darcy's law are valid in the domain of $\Phi < 1$ and $\Psi < 6 \times 10^{-3}$, allowing an error of ten percent or less in neglecting the boundary and inertia effects.

6. CONCLUSIONS

The main purpose of the present study is to show the nature and importance of the boundary and inertial effects upon flow and heat transfer in porous media. This is accomplished by first formulating the general problem with these effects present, and then applying the formulation to the specific case of two-dimensional flow through a porous medium confined by an exter-

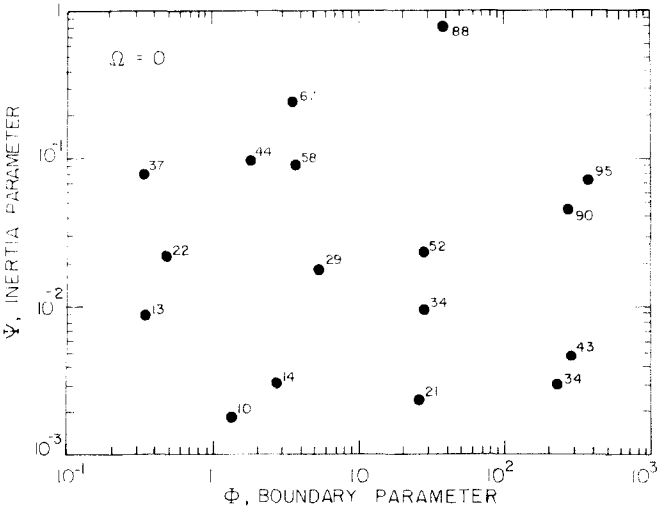

FIG. 9. The percent error on the average Nusselt number for using Darcy's law.

nal boundary. In analyzing these effects, three flow resistances must be considered: the bulk damping resistance due to the porous structure, the viscous resistance due to the boundary, and the resistance due to the inertial forces. For the flow field, the boundary effect is confined in a very thin momentum boundary layer and often plays an insignificant role in overall flow consideration. The effect of boundary on heat transfer, however, can be quite important and is more pronounced for the thermal boundary layer with a thickness less than or of the same order as that of the momentum boundary layer. This is expected to happen at high Prandtl numbers, and large pressure differences. The inertia effects increase with the higher permeability and the lower fluid viscosity. Furthermore, the velocity gradients near the wall are bound to increase, thereby increasing the viscous resistance due to the boundary. Hence, the boundary effects are further amplified as inertia increases. An error map on the basis of numerical results has been presented to illustrate the domain of applicability of Darcy's law which neglects the boundary and inertial effects.

Acknowledgements—The present work was conducted under research support from the National Science Foundation and the Department of Energy. The support to C. L. Tien by Alexander von Humboldt Foundation, Federal Republic of Germany, through a Senior U.S. Scientist Award is also gratefully acknowledged.

REFERENCES

1. A. E. Scheidegger, *The Physics of Flow through Porous Media*. University of Toronto Press, Toronto (1974).
2. P. C. Carman, *Flow of Gases through Porous Media*. Academic Press, New York (1956).
3. R. E. Collins, *Flow of Fluids through Porous Materials*. Reinhold, New York (1961).
4. E. Palm, J. E. Weber and O. Kvernvold, On steady convection in a porous medium, *J. Fluid Mech.* **54,** 153–161 (1972).
5. B. C. Chandrasekhara and D. Vortmeyer, Flow model for velocity distribution in fixed porous beds under isothermal conditions, *Thermo- and Fluid Dynamics* **12,** 105–111 (1979).
6. H. C. Brinkman, A Calculation of the viscous force extended by a flowing fluid on a dense swarm of particles, *Appl. Scient. Res.* **A1,** 27–34 (1947).
7. M. Muskat, *The Flow of Homogeneous Fluids through Porous Media*. Edwards, Michigan (1946).
8. J. C. Slattery, Two-phase flow through porous media, *A.I.Ch.E. Jl* **16,** 345–352 (1970).
9. J. C. Slattery, Multiphase viscoelastic flow through porous media, *A.I.Ch.E. Jl* **14,** 50–56 (1968).
10. G. S. Beavers and E. M. Sparrow, Non-Darcy flow through fibrous porous media, *J. Appl. Mech.* **36,** 711–714 (1969).
11. J. C. Koh, J. C. Dutton, B. A. Benson and A. Fortini, Friction factor for isothermal and non-isothermal flow through porous media, *J. Heat Transfer* **99C,** 367–373 (1977).
12. R. J. M. DeWiest, *Flow through Porous Media*. Academic Press, New York (1969).
13. C. L. Tien and K. Vafai, Statistical bounds for the effective thermal conductivity of microsphere and fibrous insulation, *Prog. Astronaut. Aeronaut.* **65,** 135–148 (1979).
14. J. C. Slattery, *Momentum, Energy, and Mass Transfer in Continua*. Krieger, New York (1978).
15. S. Whitaker, Advances in theory of fluid motion in porous media, *Ind. Engng Chem.* **61,** 14–28 (1969).

EFFETS DE LIMITE ET D'INERTIE SUR L'ECOULEMENT ET SUR LE TRANSFERT THERMIQUE DANS DES MILIEUX POREUX

Résumé—On analyse les effets d'une frontière solide et des forces d'inertie sur l'écoulement et le transfert thermique dans les milieux poreux. Une attention particulière est portée à l'écoulement à travers un milieu poreux au voisinage d'une frontière imperméable. La technique de la moyenne locale en volume a été utilisée pour établir les équations avec une indication sur les limitations physiques et sur les hypothèses. Un schéma numérique a été développé pour déterminer les champs de vitesse et de température dans un milieu poreux près d'une frontière imperméable et un nouveau concept de couche limite placé au centre de la routine numérique est présenté. Les effets de limite et d'inertie sont caractérisés par trois groupements sans dimension et ces effets sont montrés plus prononcés dans les milieux fortement imperméables, pour des fluides à grand nombre de Prandtl, pour des forts gradients de pression et dans la région proche du bord d'attaque de la couche limite de l'écoulement.

RAND- UND TRÄGHEITSEINFLÜSSE AUF DIE STRÖMUNG UND DEN WÄRMEÜBERGANG IN PORÖSEN MEDIEN

Zusammenfassung — Die vorliegende Arbeit untersucht die Einflüsse einer festen Begrenzung und der Trägheitskräfte auf die Strömung und den Wärmeübergang in porösen Medien.Besondere Aufmerksamkeit wird der Strömung durch ein poröses Medium in der Nähe einer undurchlässigen Begrenzung gewidmet. Das Verfahren der örtlichen Volumen-Mittelbildung wurde bei der Aufstellung der beschreibenden Gleichungen und der Angabe der physikalischen Vereinfachungen und Näherungen verwendet, die im Verlauf der Herleitung getroffen wurden. Für die beschreibenden Gleichungen wurde ein numerisches Lösungsverfahren entwickelt, um die Geschwindigkeits- und Temperaturfelder innerhalb des porösen Mediums nahe einer undurchlässigen Begrenzung zu untersuchen. Für die Impulsgrenzschicht wird ein neues Konzept innerhalb des numerischen Verfahrens vorgestellt. Die Rand- und Trägheitseinflüsse werden durch drei dimensionslose Gruppen ausgedrückt. Diese Einflüsse erweisen sich als stärker ausgeprägt in gut durchlässigen Medien, in Fluiden mit großer Prandtl-Zahl, bei großen Druckgradienten und im Bereich nahe der Vorderkante der Strömungsgrenzschicht.

ВЛИЯНИЕ ТВЕРДОЙ ГРАНИЦЫ И СИЛ ИНЕРЦИИ НА ТЕЧЕНИЕ И ТЕПЛОПЕРЕНОС В ПОРИСТЫХ СРЕДАХ

Аннотация — Анализируется влияние твердой границы и сил инерции на течение и теплоперенос в пористых средах. Особое внимание уделяется течению через пористую среду вблизи непроницаемой границы. Для вывода основных уравнений используется метод локального усреднения по объему. Указывается на физические ограничения и принятые допущения. С целью исследования полей скорости и температуры внутри пористой среды у непроницаемой границы разработана численная схема для решения основных уравнений и введено новое понятие пограничного слоя количества движения, являющегося основным в численной схеме решения. Влияние границы и сил инерции выражается с помощью трех безразмерных комплексов. Показано, что влияние более заметно в средах с высокой проницаемостью, жидкостях с большим числом Прандтля, большими градиентами давления и в области пограничного слоя у передней кромки.